GIS Certificate Project:

A Remote Sensing Approach to Predicting Mercury Concentration in the Great Lakes Region using Leaf Area Index

By Kim (Ness) Sundeen

Submitted as a Capstone Research Project for the Geographic Information Systems Certificate Program, University of Wisconsin-Madison, August, 2012.

Table of Contents

List of Tables

List of Figures

Abstract

Mercury is classified as a persistent bioaccumulative toxin. Sulfate-reducing bacteria, largely present in wetlands with forested landscapes, transform into its more reactive form, methylmercury (MeHg). Wet and dry deposition of Hg show varied spatial patterns of distribution and did not always positively correlate with each other. Dry deposition of Hg in the leaf litter generally positively correlated with wet deposition. Assuming that a positive association existed, we sought to use a measure of biomass to predict Hg concentration, as a form of wet deposition. We used ordinary least squares regression, with AIC_c model selection, to predict mean annual Hg concentration. Drainage basins were delineated for 40 USGS streamflow gages and used to calculate median and mean leaf area index (LAI) (for dates May to Sept, 2011), percent land cover, and percent impervious surface for the Great Lakes region. The five best models showed that only LAI from mid June (10 June) or late September (30 Sept.), along with watershed area (HUC-10) predicted just under half the variability in Hg concentration (R^2=0.44 - 0.49). Results showed a negative association between Hg concentration and LAI. The negative relationship could suggest local spatiotemporal variation of both Hg concentration and biomass. Despite wide confidence intervals of prediction, results showed higher Hg concentrations near urban areas, rising from north to south. The level of forest harvesting in these areas could play a role in increasing soil runoff and increased Hg levels as well. This study stresses how land use change (e.g., in harvested forests or urban areas) may influence potential runoff of numerous contaminants, including Hg, into nearby watersheds.

1.0 Introduction

1.1. Effects of Mercury on Great Lakes Ecosystems and Organisms

The Great Lakes Region provides 84 percent of North America's surface water and 21 percent of the world's fresh water (EPA 1995). With over 10,000 miles of shoreline that span over 201,000 mi^2 of drainage areas (EPA 1995), these vast freshwater natural resources provide recreation, employment, food, and water to more than 35 million people (Evers et al. 2011b). Given the reach and influence of the Great Lakes, water quality is critical to ensure a healthy ecosystem. Monitoring the water quality is important for ensuring contaminant levels do not exceed certain standards.

The threat of mercury (Hg) continues to affect the health of the Great Lakes Region. Although a naturally occurring element on earth, in large concentrations, Hg can pose serious problems in the environment and to human health. Human activities are estimated to release up to two-thirds of Hg globally (Mason et al., 2005; UNEP Chemicals Branch, 2008). High amounts of Hg were used in industry for its diverse properties, but its use declined precipitously by the mid 1990's after widespread elimination of Hg from pesticides (EPA, 1995). Mercury is also released into the atmosphere when it is burned. In the US, anthropogenic sources from coal-burning power plants account more than 50 percent of US Hg emissions (EPA, 2005).

Since 2007, five states have issued consumption advisories from high levels of mercury (Hg) in common freshwater fish (Evers et al., 2011b). This is classified as a persistent bioaccumulative toxin by the Environmental Protection Agency (EPA) (EPA, 2001). Overconsumption of fish with high levels of methylmercury (MeHg) can have adverse and unknown effects on the brain and nervous system such as seizures or mental retardation (Silbernagel, 2011). There are subtle neurological and reproductive effects in humans and wildlife caused by consuming Hg-

contaminated fish (Gilbertson and Carpenter, 2004). After mercury has traveled to wetland systems, sulfate-reducing bacteria transform elemental Hg to MeHg (Sørensen, et al., 2009). As larger predators consume Hg-laden prey, higher levels of Hg bioaccumulate in organ tissue of animals such as common loons or walleye (Evers et al., 2011b). In turn, the level of Hg consumed by larger predators biomagnifies up through the food chain. Piscivorous fish such as walleye and northern pike (favorites among anglers), have increased MeHg concentrations (Evers et al. 2011a). This amplifies the risk to humans consuming such fish.

Initial regulation, beginning around the 1970's, addressed Hg deposition in the Great Lakes from large industrial sources such as paper and pulp mills (Evers et al., 2011b). During this period, under the Boundary Waters Treaty Act of 1909, the International Joint Commission was established to assist the US. in implementing the 1978 Great Lakes Water Quality Agreement (EPA, 1989). This Commission made mercury a priority concern for several reasons: the availability of emerging predictive Hg cycling models, the EPA's decision in 2000 to decrease the reference dose of Hg to 0.1 µg/kg body weight/day and the increasing number of fish consumption advisories across the Great Lakes (Gilbertson & Carpenter, 2004). Despite this priority designation, Hg remains a major threat to humans and Great Lakes ecosystems 30 years later.

1.2. Distribution of Mercury

The majority of Hg deposition is atmospheric, making it difficult to where Hg originated. For example, when Hg is emitted as gas and particles, it can travel up to 10 km from the original stationary source (Driscoll et al., 2007). Atmospheric Hg is transported from point sources to the environment as wet and dry deposition. Wet Hg is deposited to ecosystems through precipitation, whereas dry deposition is the process of Hg transfer from atmosphere to the terrestrial surfaces (Risch et al., 2011).

Watersheds that have received elevated levels of Hg are considered mercury-sensitive watersheds. These watersheds are densely forested with numerous wetlands (Evers et al., 2011a). In these areas, litterfall (i.e., biomass) may become another major source of Hg through dry deposition in dense forest stands, such as those in the northern reaches of the Great Lakes states. A study across the eastern U.S. showed that even in forested landscapes with moderate wet Hg deposition, high levels of dry deposition can occur (Risch et al., 2011). The spatial pattern indicated an increase in litterfall Hg from Georgia northward through Wisconsin and New York. Another study of fish Hg concentration in the Great Lakes revealed a similar trend of increasing Hg levels south to north, with higher levels in the eastern compared to western Great Lakes region (Monson et al., 2011).

These studies suggest that not considering both the dry and wet forms of Hg depositions fails to accurately portray the distribution of Hg across the landscape. Although higher dry deposition correlates with higher point-source mercury deposition points, regional-scale studies also suggest that few patterns occur in atmospheric Hg wet deposition (Engle et al., 2010). Nevertheless, numerous studies attempt to estimate total Hg through landscape-scale and catchment-scale models.

Regional studies provide the spatial patterns to understand local Hg cycling (Driscoll et al., 2007; Engle et al., 2010; Gilbertson & Carpenter, 2004). Local studies provide the more detail review of additional variables that affect Hg cycling (Hurly et al., 1995; Babiarz et al., 2012; Zhang et al., 2012). Empirical models of Hg cycling provide predictions of total Hg or MeHg at the basin-scale catchment (Futter et al., 2012; Brakebill et al., 2011). However, more research that provides

ecosystem-scale analysis of total Hg distribution (Lindberg et al., 2007; Mason et al., 2005) is needed, especially in evaluating the empirical models.

Similar broad-scale studies of landscape factors affecting water quality have provided insight into ecosystem processes. Forest cover such as the particular tree species, canopy density, and leaf area influence the amount of precipitation partitioned in remaining in the canopy leaves as precipitation storage and net precipitation reaching the forest floor (Winkler et al., 2009). We might expect increased Hg in watersheds in areas with more net precipitation due to storm events or harvesting. Extending this to urban environments with higher impervious surface or fewer forests, more net precipitation would reach nearby watersheds. Additionally, studies have shown that forest harvesting can increase snow accumulation and eventual elevated snowmelt (and wet deposition) of contaminants streams (Murray & Buttle, 2003; Winkler et al., 2005).

A review of the effects of forest removal on streamflow emphasized the fact that in areas with reduced forest cover (i.e., biomass), streamflow increased (Buttle & Murray, 2011). Organic soils such as those in boreal forests accumulate more Hg (Dersrosiers et al., 2006). Following forest cover removal, favorable environmental conditions for sulfate-reducing bacteria (e.g., increases in soil temperature, water tables, and the availability of carbon) amplify Hg methylation (Sørensen, et al., 2009). This is the basis of my research, with the research objective to quantify the relationship between upstream biomass and downstream hg accumulation.

To accurately estimate the accumulation of basin-wide Hg, long-term monitoring of stream mercury is needed. Without these data however, known relationships between biomass and Hg can serve as indicators of Hg across a larger landscape. Concentrations of Hg have increased in lakes and streams with higher abundance of forests and wetlands farther north (Evers et al., 2011a; Engle et al., 2010). I sought to add to the current literature investigating the relationship between watershed-measured Hg concentration and remotely-sensed LAI.

1.3. Research Objective

Given this previous positive relationship between forest and wetland landscapes with Hg levels, this study's research objective was to test whether biomass would show a positive relationship with Hg concentrations measured at U.S. Geological Survey (USGS) gauge stations. To meet this objective, I collaborated with researchers at the USGS Water Science Center in Middleton, WI to develop research questions and a methodology to predict Hg concentration. Upstream biomass was measured as leaf area index (LAI) while downstream Hg accumulation was measured from USGS streamflow gages.

As an important measure of forest canopy, LAI provides the three-dimensional aerial coverage of leaves measured as area per unit ground-surface area (Jenson, 2006). Field collection of biomass is time intensive, which involves estimating leaf area from destructive leaf sampling (Jonckheere et al., 2004). The samples are dried and weighed to determine the number of aerial units covered by leaves in a horizontal plane. Less time-intense indirect leaf area estimation is based on the spectral response of active radiation from seven spectral bands collected from satellite images. The bidirectional reflectance distribution function (BRDF) is calculated from solar azimuth and zenith angles recorded by satellites. This BRDF describes the bidirectional characteristics of the sun's irradiance and the angle of the remote sensor viewing the feature of interest (Jenson, 2006). A widely-used and well-documented LAI produced is produced from the Moderate Resolution

Imaging Spectroradiometer (MODIS) satellite imagery. MODIS LAI product is created using spectral imagery retrieved By accounting for BRDF angles, a measure of the three-dimensional forest canopy structure (i.e., LAI) is created from compression algorithm that reduces redundant information to one spectral response, interpreted as LAI (Myneni et al., 2003). The reader is referred to the MODIS user guide on LAI for more background on the LAI algorithm (Myneni et al., 2003; Knyazikhin et al., 1999).

2.0 Methods

This study's aim was to develop inferential models for predicting future Hg Concentration for the entire Great Lakes Basin. A unique spatial analysis at the time, Hurley (1995), took advantage of previously-established relationships between land cover and stream water quality. Models that make use of large datasets to predict regional-scale nutrient estimates (e.g., SPatially Referenced Regressions on Watershed Attributes "SPARROW" [Schwartz et al., 2006] and Soil and Water Assessment Tool, "SWAT" [Neitsch et al., 2011]). This study makes use of only the Great Lakes region to investigate relationships of Hg concentration and landscape variables. Specifically, this method involved identifying empirical relationships between several landscape-scale variables and Hg Concentration in the Great Lakes drainage basins with the additional parameter of remotely-sensed LAI.

2.1. Study Area

The study area was centered on the Great Lakes Region Basin, as defined by the USGS National Hydrography Dataset (NHD), Hyrdologic Unit Code 04 (HUC-04), which borders the United States of Minnesota, Wisconsin, Illinois, Indiana, Ohio, Michigan, Pennsylvania, New York, Vermont, New Hampshire, and Maine and Canada's provinces of Ontario and Quebec. The extent of the Great Lakes Region is 49.022615°N, -93.213865°W and 40.394681°N, -70.238450°W (North American Datum 1983).

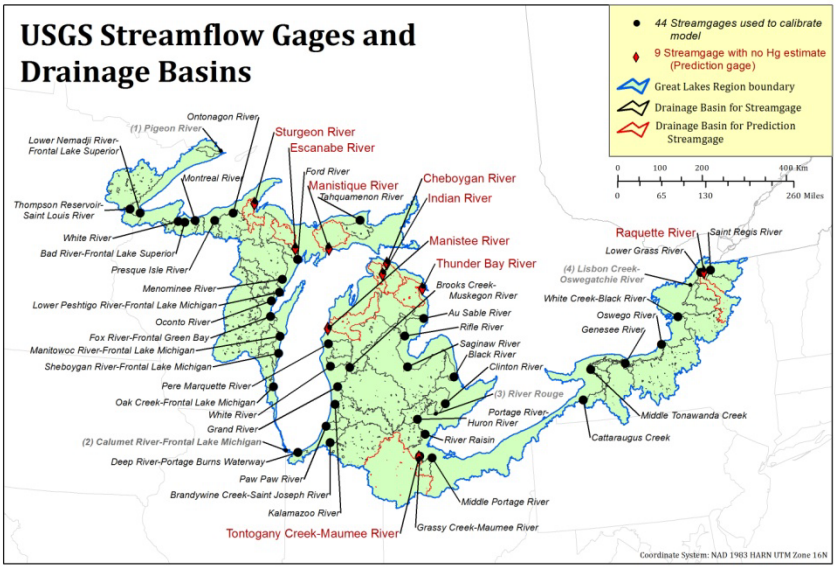

Figure 1. Study area map with streamgages used for model calibration (black points) and nine prediction streamgages (red diamonds).

2.2. Variables for Regression Model

To build upon this initial landscape-scale research, USGS collaborators and I analyzed data recorded daily over the full 2011 hydrologic year at 53 USGS streamflow-gaging stations (hereafter "streamgage") located in five states bordering the Great Lakes (Figure 1,2). Using a set of candidate log-linear multilinear regression models, I predicted Hg concentration from the algebraic combination of these several relevant predictor variables. I evaluated the significance influence of total flow, basin drainage area, watershed area, LAI, and land cover for predicting Hg concentration. Except for watershed area, I measured each predictor variable at the scale of the streamgage and Drainage Basin. I listed all variables in Table 1 deemed important in understanding what influences Hg Concentration spatially. The definitions and source are listed in Table X as well.

2.2.1. Response Variable: Mercury Concentration

For the response variable, I estimated the mean daily Hg concentration for each streamgage for 2011. Streamgages recorded hourly water quality and streamflow values. I decided to use this mean value because it provided an overall value and reduced extremes of flow and Hg Concentration. Fifty-three streamgages were available that had Hg concentration values. Two streamgages only had mean Hg Concentrations for 61 and 92 days of the year. Because of the relatively large sample size, I included these streamgages in the model. However, nine streamgages had missing Hg Concentrations, two had technical errors in calculating Drainage Basins, and two had null values for LAI, thus leaving 40 streamgages for calibrating the regression model.

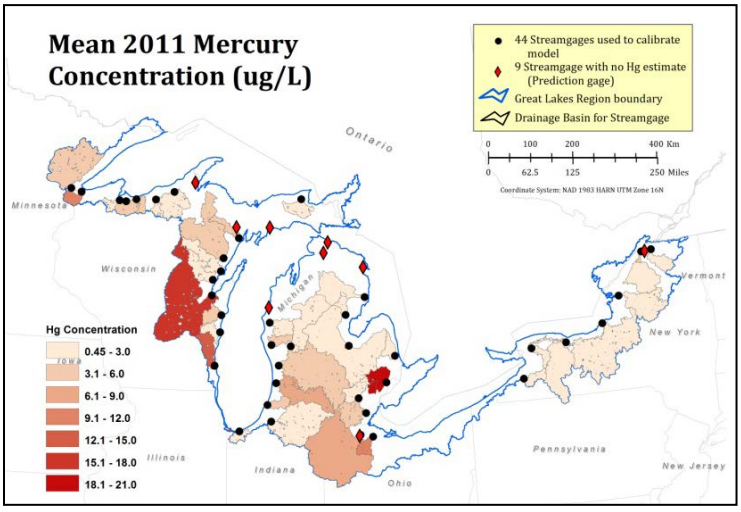

Figure 2. Distribution of mean annual Hg concentration enumerated by drainage basin.

Table 1. List of response and predictor (i.e., independent) variables.

Model Variable	Model Variable	Definition	Data Range	Units	Data Source
Response	Mercury Concentration*	Mean daily Hg concentration, as summarized from hourly measurements of 53 streamgages 2011, over the 365 days.	0.448 – 19.151	µg/L	USGS, Streamflow-gaging stations
Predictor: streamgage	Total Flow**	Mean daily flow of water averaged for 2011, over the 365 days. The sum of all contributing streamflow sources (base flow, direct runoff, and discharge [Carter et al., 2005])	4,213-3,760,489	Liters	USGS, Streamflow-gaging stations
Predictor: Basin-level	Drainage Area**	Entire drainage area of a watershed upstream of a USGS gaging station (calculated from digital elevation models of flow accumulation; calculated for each USGS gauge; these include overlapping in Drainage Basins.	261 - 6,330	Miles^2	USGS, ArcHYDRO model of basin delineations
	HUC_10*	Areas of watershed that drains were linked to the USGS gauge site as a local measure of the drainage to the gauge.	52.06 - 389.14	Miles^2	USGS, Watershed Boundary Dataset (WBD)
	LAI(date)*	Mean and Median of Leaf Area Index (LAI) estimated within the Drainage Area. This is the 3D measure of biomass in a forest canopy. Dates were measured from Julian date 129 (May 9th) to 273 (Sept 30th)	0 - 6	Unitless	NASA, 2011
	Broad Land Cover Types*: AllForest AllWetland AllCrops AllDeveloped	Percent land cover was calculated from 2006 National Land Cover Dataset (NLCD) estimated within the Drainage Area.	0 - 100	Percent Land Cover	Fry et al., 2011
	***Specific Land Cover Types**:* PastureCrops CultivatedCrops EvergreenForest MixedForest DeciduousForest OpenWater EmergentWetland WoodyWetland		0 - 100	Percent Land Cover	Fry et al., 2011
	Impervious Surface*	Mean percent impervious surface estimated within the Drainage Area, extracted from the 2006 National Land Cover Dataset Impervious Surface product.	0 - 100	Percent Impervious Surface	Fry et al., 2011

*Continuous (float) data type
**Continuous (integer) data type

2.2.2. Predictor Variables

USGS Streamflow Gage Measurements

At the USGS gauge scale, I only measured total flow and Hg concentration. Total flow (L/yr) (Figure 3) provided an estimate of the total volume of water flowing passed each gauge for the entire year. Hg concentration (ng/L) as the dependent variables in the regression models. Previous attempts were made to predict Hg yield and Hg load, yet due to collinearity, these variables were dropped as response variables. A standard method of estimating Hg Yield involves estimating the aerial input of Hg into the watershed (Carter et al., 2005) measured as micrograms per area (μg/mi^2). Total Load is estimated as the total mass (grams) of a contaminant feeding into a stream (Carter et al., 2005). Due to the variation of methods for estimating Yield and Load, the decision was made to only model Hg Concentration measured because Total Flow was highly correlated with both Hg Load and Hg Yield; thus these two variables were removed from further analyses.

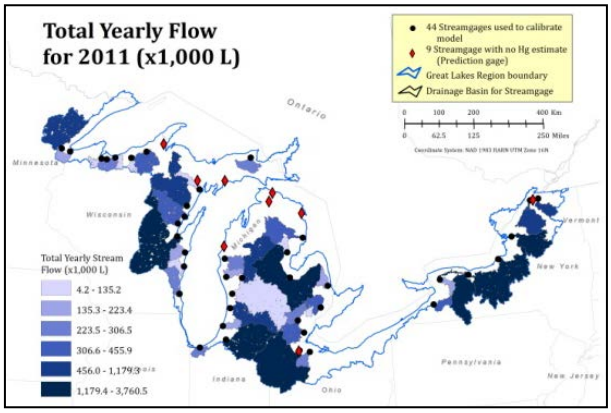

Figure 3. Distribution of mean annual streamflow enumerated by drainage basin.

Hg concentration is more logical to model for this current study because the larger goal is to model future climate change with the USGS Precipitation Runoff Modeling System (PRMS) (Walker, J., pers. comm., 26 June 2012). This PRMS may potentially use this study's results to predict future Hg Load. Therefore, Hg Load is not necessary to accurately estimate Hg concentration in place of Hg load and Hg yield.

Drainage Basins for Streamgages

To estimate landscape variables at the scale of the Great Lakes Region, I used an enumeration unit (i.e., aggregation unit) of each gauges' drainage basin (Figure 1). This spatial unit was necessary to obtain landscape-scale statistics of the LAI and land cover for each USGS gauge. The drainage area represented the area (mi^2) containing all streams that flowed into each gauge. These results were analyzed to ensure that the linear regression assumptions were not violated since some variables overlapped. Because of the spatial aspect of this research, by including this overlap the variables could account for the spatial dependency the drainage basin and LAI. Tobler's (1970) first law of geography stated that "Everything is related to everything else, but near things are more related than distant things." With any geographic phenomenon, I expect that nearby measurements will have values closer to those of their neighbors than values from farther away.

The USGS National Hydrography Dataset (NHD) (USGS & EPA, 2012) provided the framework for delineating drainage basins for each USGS gauge. This dataset was ideal for aggregating the LAI and land cover variables for their relationship to the georeferenced stream network of directionally-attributed "flowlines." Additionally, these data referenced six "Watershed Boundary" levels,

offering the potential for multi-scale comparisons of landscape variables. For example, I could measure LAI at the watershed level (i.e., HUC 10) and compare the effect of scale at the sub-basin level (i.e., HUC 8) (USGS & USDS NRCS, 2012).

Each streamgage measured streamflow characteristics from the upstream streams. These streams pass through landscapes with varied land cover types, soil, and urban development. To capture this upstream landscape information, I needed to quantity the area that drained into streamgages. I would then use this Drainage Basin as the enumeration unit to summarize the percent land cover type, percent impervious surface (as a measure of urbanized area and potential for runoff), and LAI.

My goal was to use stream networks to highlight upstream catchments that fed into each streamgage. Catchments, the smallest landscape drainage area, were calculated using a flow-accumulation method (Schäuble et al., 2008). The slope of a digital elevation model gives the flow direction, from which stream fill and accumulation were estimated (Arnold, 2010). Aggregating all the catchments along a stream to a particular streamgage results in the Drainage Basin.

To calculate the Drainage Basin for streamgages, I first used a publically-available *Basin Delineator* tool (Horizons Systems Corporation, 2006). However, due to technical errors with this tool running on an ArcGIS 9.3 platform, only 22 of the 44 streamgages were delineated. To circumvent these errors, I used a manual basin delineation method for two reasons. First, I sought to test the Drainage Basin results of this manual method with the results of the *Basin Delineator* tool. Second, because the *Basin Delineator* tool was developed for an earlier and relatively out-of-date flowline dataset (e.g., 2006), I preferred to use more recent flowline and catchment data. Flowlines are digitized vector streams, attributed with flow direction, enabling estimation of the upstream and downstream locations. More specifically, with the July 2012 release of the NHDPlus version 2 (Horizon Systems Corporation, 2012), I used these data to estimate upstream flow accumulation to aggregate catchments.

For my manual drainage basin delineation method, I used the NHD, version 2, "high" resolution (1:24k) flowline data for the Great Lakes Region by Hydrologic Unit (HU) 4 through 15 subregions. These flowlines provided more detailed stream characteristics than the NHDPlus flowlines did in the "medium" resolution (1:100K) data. Using the *ArcGIS* (ESRI, 2011), "Utility Network Analyst", I manually delineated the networks using the "upstream flow accumulation" option. The added benefit to using NHD alongside the NHDPlus was utilizing the catchment, which was calculated from the flowlines of the NHD.

Results of the upstream accumulation along NHD flowlines highlighted NHDPlus catchment features. I aggregated these catchments and linked them to each streamgage. Of the 44 drainage basins, 42 were within 100 mi^2 of the original drainage area used to estimate Hg concentration and total flow. In comparing the original "Hydrologic Response Unit" (HRU) drainage area from PRMS models (Walker, J., pers. comm., 26 June 2012), I only used drainage basins that were within 100 mi^2 of HRU drainage areas. As a result, I discarded two drainage basins I delineated from analysis that differed in area.

Watershed Area for Streamgages

As a smaller scale and independent measure of the hydrologic area, I used the Hydrologic Unit Code (HUC), level 12, for the subwatershed area around each streamgage. The HUC boundaries are known as Watershed Boundary Datasets (WBD), for which the USGS delineates hydrologic boundaries of six levels. Each level is designated by its HUC between two and 12 digits (Figure 4). Regions—the largest watershed level—have two digits to indicate one of 21 Regions across the US.

The smallest watershed level is the subwatershed designated with a 12-digit HUC. The watershed level, HUC-10 was the unit of analysis for this study. I used the HUC-10 area as a variable as a way to standardize the local variation. The HUC-10 provided a readily-available measurement that could also be used for applying to unmeasured areas to measure Hg Concentration. I used the area of these HUC-10 boundaries as an indicator of local watershed variation and linked these data to the streamgage (Figure5).

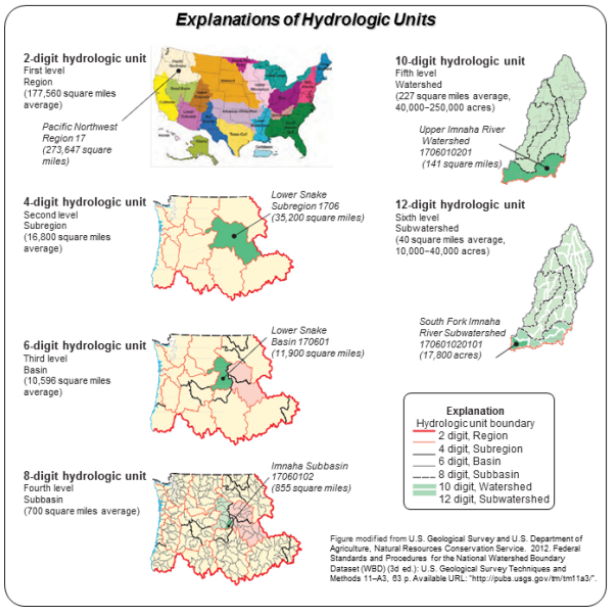

Figure 4. Graphical description of Hydrologic Units and respective Codes for each hydrologic level.

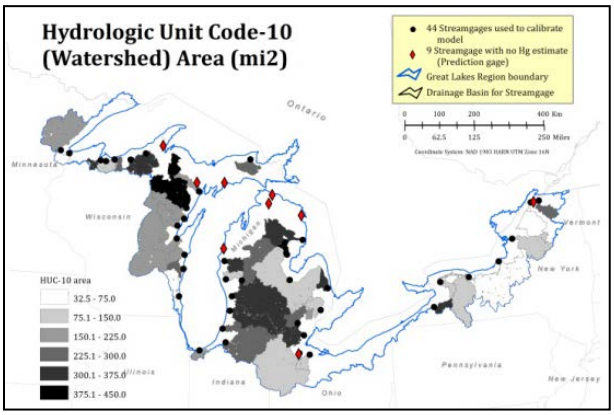

Figure 5. Distribution of watershed (HUC-10) area.

Biomass Estimation: Median of Drainage Basin

I used the MODIS LAI data products as the estimate of biomass. I downloaded all MODIS Download and extracted weekly LAI MODIS 250m resolution satellite images (grid locations "v4h12" and "v4h11") for general growing season dates April to September 2011 (NASA, 2011). Because of the small geographic scale (1:10,000,000) of this study, higher resolution data was not necessary for estimating local and regional LAI estimates, and the 250-m spatial resolution of MODIS images was convenient and simple to process. Additionally, as other satellite images often require hours of pre-processing to correct atmospheric interference, this MODIS LAI data product downloads in a pre-processed format with atmospheric correction.

MODIS data were developed through a collaboration of researchers and validated with ground-measured LAI. These LAI products have been validated in studies by numerous international research teams in over 20 locations across the world from France to the Kalahari Dessert in Africa (Yang et al. 2006). Considering all six biomes worldwide that were sampled areas for the evaluation of LAI, estimates suggest that LAI potentially overestimates LAI by 12%. However, for the evaluated site in Wisconsin, ground LAI estimates only differed from MODIS LAI estimates by seven percent (Ahl et al., 2006). The six maps in Figure 6 represent the raw LAI data (left maps) compared with the LAI summary statistics, aggregated by drainage basin.

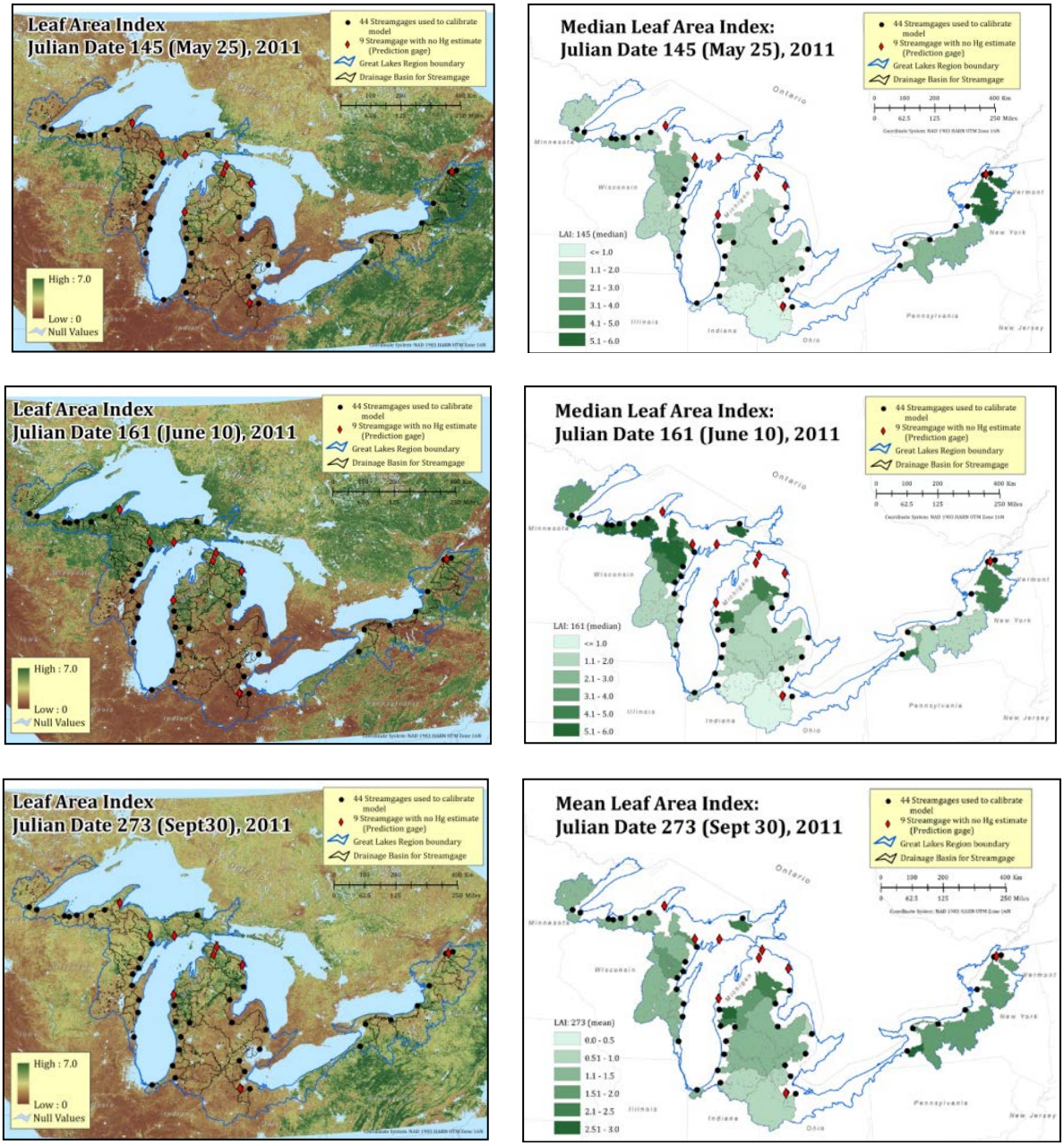

Figure 6. Distributions of MODIS Leaf Area Index (LAI) estimates for three dates: 5/25/11, 6/10/11, and 9/30/11. Left images are continuous surfaces of LAI. Right images are LAI measurements summarized by median or mean value within the streamgage Drainage Basin.

Land Cover Estimation: Percent of Drainage Basin

I estimated percent land cover within basins by converting all land cover in the 2006 National Land Cover Dataset (Fry et al., 2011) to binary variables. For each land cover type (e.g., all forest type or emergent wetland), I reclassified all land cover types to either "1" for the land cover of interest, or "0" if not. I then calculated the mean of these 1's and 0's and divided it by the basin area. This gave me the percent of land cover within the basin for USGS gauges (Figure 7).

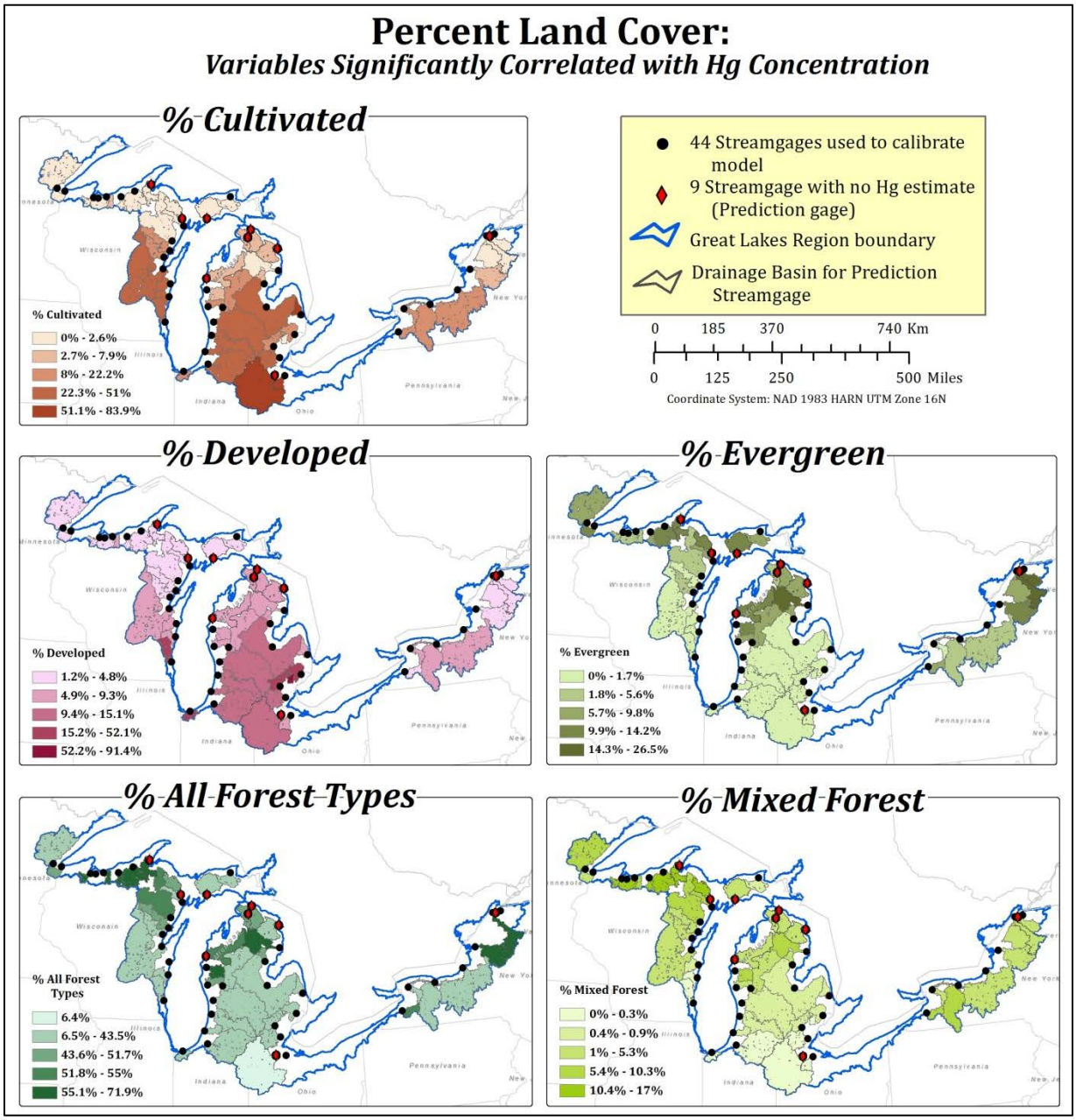

Figure 7. Distributions of percent landcover averaged by drainage basin for USGS streamgages. Distributions are displayed with Jenks classes to allow comparison across all maps.

Percent Impervious Surface: Mean Percent of Drainage Basin
Impervious surface typically describes artificial structures such as concrete or rooftops. This is a useful indicator of urbanized areas. The Multi-Resolution Land Characteristics Consortium (MRLC) also provides a data product that estimate percent impervious surface. I estimated the mean percent impervious surface within Drainage Basins for streamgages (Figure 8).

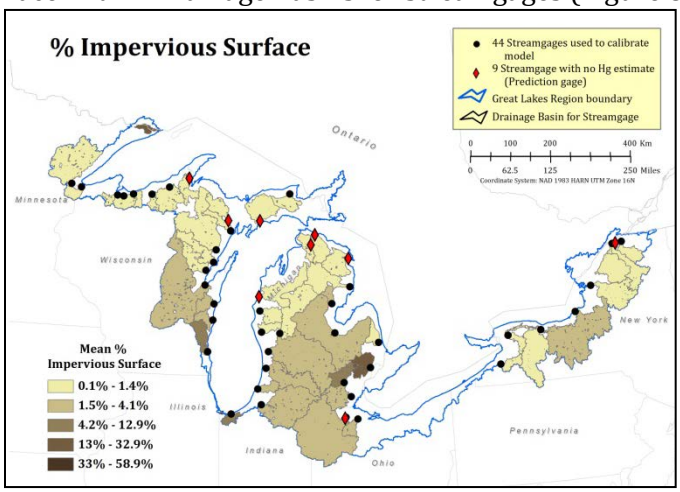

Figure 8. Distribution of percent impervious surface averaged by drainage basin. Distributions are displayed with Jenks classes to allow comparison across all maps.

2.3. Regression Analysis

2.3.1. Model Calibration

My goal was to use the 100 predictor variables and identify the best variables for predicting Hg concentration. I fit the model using ordinary least squares estimation. In comparing the results of the candidate regression models, I used two statistical programs to compare the output of the AICc selection process including *Virtual Beach* (Center for Exposure Assessment Models) and *R (*R Development Core Team). I used the resulting model to build an ordinary least squares regression ("OLS") tool in *ArcGIS* (ESRI, 2011). I prepared the data in the same manner for input into all three software packages: *Virtual Beach, R, and ArcGIS*. I ran the first analysis in *Virtual Beach*, a free statistical tool for multilinear regression models, developed by the Environmental Protection Agency for assessing beach water quality and pathogen exposure. My second analysis involved using a stepwise automated AIC_c model selection algorithm to compare results with those of Virtual Beach. I used the "glmulti" package in *R*, version 1.15.

To follow the regression assumptions of normality, I transformed most variables (x) to increase the linear associations with the response variable, Hg concentration, using logarithmic (log10[x]), inverse (1/x), square, or square root ($\sqrt{x}$). I used these transformations to increase the linearity between all predictor variables. These transformations also improved the model fit by normalizing residual errors. *Virtual Beach* was used to automate the data-mining process of building multiple linear regression models for hundreds of thousands of candidate models. The automated process runs analysis of all models and only selects models based on a user-specific model selection criterion (e.g., AIC_c or R^2) and constraining models with less multicollinearity (e.g., using a low variance inflation factor (VIF)). Another benefit of running this software was the options for iteratively assessing the prediction accuracy of each model using cross-validation and testing the mean square error of prediction (MSEP).

Model Selection

To select the most parsimonious models, I used multiple log-linear regression, using the corrected Akaike Information Criterion (AIC_c) model selection to identify the best fit models. The method assigns higher weights to more parsimonious models and thus penalizes models with a large number of predictors, which reduces model overfitting.

AIC_c weights are the relative likelihood that a model is the best given the parameters of the model. This is based on. Likelihood is the probability of the observed results given the model predictor variables. AIC_c uses maximum likelihood estimation to maximize the likelihood function of the given model with a set of variables. Relative likelihood of the given models is calculated using $e^{(-0.5 * \Delta AIC \text{ model score})}$. Therefore, the Corrected Akaike weight for each model is the relative likelihood divided by the sum of all model maximum likelihood.

To automate the model selection process in *R*, I used backward selection because it is considered more robust than forward selection and less susceptible to collinearity (Chatterjee & Hadi 2007, p 290). Backward selection allowed comparison of AIC_c weights between candidate (i.e., "nested") models. I only retained candidate models with variables that added significantly to predicting the response variable according the Wald test results of AIC_c weights between the full (i.e., included all variables) and reduced models (i.e., included only significant variables).

In Virtual Beach, I set parameters to automate the process of selecting models using AICc criteria. I only allowed five predictor variables be included in final models. I set the maximum VIF at 3 to reduce multicollinearity in final models. With the final ten models, I used the cross validation option to iteratively assess the prediction accuracy with the mean square error of prediction (MSEP).

I only included the top five models with a change in AIC_c (ΔAIC_c). I retained models with $\Delta AIC_c < 2.0$ where the ΔAIC_c is the difference between that model and the most parsimonious model as suggested by Burnham & Anderson (2006, p 70). I present results as AIC_c weights as the likelihood of the model given the data. My smaller sample size (n=40) warranted my use of second-order AIC_c selection equation shown below from Hurvich & Tsai (1989):

$$\boldsymbol{AIC} = n \left(\ln \left(\frac{RSS}{n}\right) \right) + 2K$$

$$\boldsymbol{AIC_c} = n \left(\ln \left(\frac{RSS}{n} \right) \right) + 2K \left(\frac{K+1}{n-K-1} \right)$$

Where:

RSS *= residual sum of squares of regression.*
K *= number of parameters (predictor variables) included in a model*
n *= sample size*
$\boldsymbol{ln}\left(\frac{\boldsymbol{RSS}}{\boldsymbol{n}}\right)$ *= the natural log-likelihood of the model, given the data*

Evaluation of Model Fit and Regression Assumptions

For model diagnostic tests, I assessed model fit by testing all assumption of linear regression. I used a Neyman smooth global test of linear assumptions and performed specific directional tests designed to detect skewness, kurtosis, a nonlinear link function, and heteroscedasticity. I tested nonlinearity, looking at patterns in graphed and mapped residuals, the R^2, variance inflation factor

(VIF) for mulitcollinearity, and confidence intervals of coefficients. A final step in selecting the best models involved measuring the relative predictive accuracy of each model using the mean-squared error of prediction (MSEP). The MSEP is measured as the Euclidean distance between the predicted Hg concentration and the expectation (i.e., observed) Hg concentration estimate. Because this study's goal is prediction, I wanted to find models that minimized this error between observed and expected Hg concentration (Brinda 2012). I ranked all models by MSEP and listed the top five models.

The VIF gives the indication of mulitcollinearity of predictor variables in a regression. The VIF measures how much a predictor variable's variance is increased by the presence of a linear association between two predictor variables. Inflated variance leads to wide confidence intervals of the estimated coefficients and thus makes prediction difficult (Cyterske et al., 2012). In a given equation with two collinear variables, a VIF value of ten or higher suggests multicollinearity and can cause estimation problems.

I also tested if the residual between observed and predicted measurements were spatially autocorrelated. I used a global test of spatial autocorrelation, Global Moran's I, to assess the spatial associations of nearby measurements. This measure is essentially the spatially-weighted equivalent of Pearson's correlation coefficient (Waller & Gotway, 2004). The spatial weight refers to a distance measure between measurements. Neighboring points have weights closer to 1, whereas farther points take on a value of 0. In Moran's I formula (Moran, 1950) below, the w_{ij} indicates the distance-weight between two observations i and j. Thus, the *I* statistic is the sum of the weights between every pair of locations measured.

$$I = \frac{n}{S_0} \frac{\sum_{i=1}^{n}\sum_{j=1}^{n} w_{ij}(x_i - \bar{x})(x_j - \bar{x})}{\sum_{i=1}^{n}(x_i - \bar{x})^2}$$

Where:

$\boldsymbol{w_{ij}}$*= residual sum of squares of regression.*
$\boldsymbol{I}$ *= number of parameters (predictor variables) included in a model*
$\boldsymbol{j}$ *= sample size*
$\boldsymbol{x_i}$ *= location i of variable x (measured here as a residual)*
$\boldsymbol{x_j}$ *= location j of variable x (measured here as a residual)*
$\boldsymbol{S_0}$ *= the sum of all weights for each pair (below)*

$$S_0 = \sum_{i=1}^{n}\sum_{j=1}^{n} w_{ij}$$

2.3.2. Prediction of Hg Concentration at Un-Measured Locations

Nine streamgages (Figure 1 and Figure 2) lacked Hg concentration data and were therefore ideal candidates for testing each model's predictive accuracy. For these streamgages, I measured predictor variables to predict Hg concentration using all five best-fit models.

3.0 Results

3.1. Significant Predictor Variables

Variables that highlight correlated with Hg concentration (e.g., r > 0.4) tended to be included in regression models. Only variables with r>=0.3 were included in the model selection stage. These significant variables are listed in Table 2.

Table 2. Pearson's correlations between all predictor variables and response variable Log10(Hg concentration). "Variable Transformation" gives the specific transformation used to increase linearity with the response variable. "Date" lists the calendar date for Leaf Area Index (LAI) Julian dates. Under "Variable Names," all predictor variables are listed that had significant correlations (r≥0.3) with the predictor variable.

Variable Transformation	Date (for LAI)	Variable Name	Pearson's Product Moment (r)	p-value
SQUARE		**Area of Hydrologic Response Unit**	0.2599	0.1053
INVERSE		**Area of Hydrologic Unit Code-10**	0.5027	0.0009
INVERSE	9-May	**LAI_129_MD**	0.3767	0.0166
INVERSE	9-May	**LAI_129_MN**	0.3613	0.0220
LOG10	17-May	**LAI_137_MD**	-0.4004	0.0105
SQUARE	17-May	**LAI_137_MN**	-0.3640	0.0210
INVERSE	25-May	**LAI_145_MD**	0.3128	0.0494
INVERSE	25-May	**LAI_145_MN**	0.3273	0.0392
INVERSE	2-Jun	**LAI_153_MD**	0.3623	0.0216
INVERSE	2-Jun	**LAI_153_MN**	0.3565	0.0240
INVERSE	10-Jun	**LAI_161_MD**	0.3081	0.0531
INVERSE	10-Jun	**LAI_161_MN**	0.3255	0.0404
INVERSE	26-Jun	**LAI_177_MD**	0.3543	0.0249
INVERSE	26-Jun	**LAI_177_MN**	0.3445	0.0295
INVERSE	4-Jul	**LAI_185_MD**	0.3658	0.0203
INVERSE	4-Jul	**LAI_185_MN**	0.3553	0.0245
INVERSE	12-Jul	**LAI_193_MD**	0.3997	0.0106
INVERSE	12-Jul	**LAI_193_MN**	0.4027	0.0100
INVERSE	28-Jul	**LAI_209_MN**	0.3013	0.0589
INVERSE	13-Aug	**LAI_225_MD**	0.3443	0.0296
INVERSE	13-Aug	**LAI_225_MN**	0.3273	0.0392
LOG10	30-Sep	**LAI_273_MD**	-0.4544	0.0032
LOG10	30-Sep	**LAI_273_MN**	-0.5116	0.0007
SQUARE		**% Cultivated**	0.2956	0.0641
SQUARE		**% Developed**	0.3269	0.0395
SQUARE ROOT		**% Evergreen**	-0.3954	0.0116
INVERSE		**% All Forest Types**	0.3444	0.0295
SQUARE ROOT		**% Mixed Forest Type**	0.2757	0.0851

3.2. Model Calibration

3.2.1. Model Selection

I only report the model results from Virtual Beach because the top five models produced from the algorithm in *R* included variables with significantly high VIF values, while Virtual Beach automatically filtered such models out. For example, the fifth best model *R* output included the land cover variable of percent of all forest types. This variable, however, highly correlated with LAI 273 (r= 0.729), which logically confirmed that LAI is another measure of forest cover, being the three-dimensional measure of forest canopy. The five best-fit models (Table 3) had the lowest MSEP, with the smallest squared difference between the observed and predicted value. These models had R^2 values between 0.446 to 0.487. "Model 1" explained most of the variance. For a full description of each model's coefficients, see the Appendix.

Table 3. Diagnostic tests of top five best-fit models, ranked by mean square error of prediction (MSEP). Most parsimonious models had the lowest AIC_c weight.

Model Number	AIC_c Weight	ΔAIC_c	MSEP	R^2	Adjusted R^2	Variables
Model 1	-53.7851	0.0000	0.0908	0.4872	0.4445	*INV(HUC-10-area) + log10(LAI-273-mean) + INV(LAI-161-median)*
Model 2	-53.2996	-0.4856	0.0927	0.4458	0.4159	*INV(HUC-10-area) + log10(LAI-273-mean)*
Model 3	-51.722	-2.0632	0.0938	0.4601	0.4151	*INV(HUC-10-area) + log10(LAI-273-mean) + INV(LAI-145-median)*
Model 4	-52.9103	-0.8749	0.0941	0.4759	0.4322	*INV(HUC-10-area) + log10(LAI-273-mean) + INV(LAI-161-mean)*
Model 5	-51.9635	-1.8216	0.0943	0.4634	0.4186	*INV(HUC-10-area) + log10(LAI-273-mean) + INV(LAI-145-mean)*

3.2.2. Evaluation of Model Fit and Regression Assumptions

The top five models (Table 3) included several LAI terms. As the top model ("Model 1") included two LAI terms, I checked for possible interaction between these terms, since the presence of collinearity would inflate the model significance. Although the interaction term had a significant linear association with log10(Hg Concentration) (r = -0.3516, p-value = 0.0261), the slope of the interaction term was not significant (t=1.34, p-value=0.189) (Table 4).

Table 4. Results of model with interaction terms of LAI 273 (median) and LAI 161 (median). Model had a R2 = 0.4949 and adjusted R2 = 0.4371, and p-value <0.000.

Parameter	Coefficient	Std. Error	t-Statistic	P-Value
(Intercept)	2.0646	0.3130	6.597	<0.0000
INV(HUC-10-area)	43.5120	10.7015	4.066	0.0003
LAI-273-mean	-0.7402	0.2538	-2.917	0.0006
LAI-161-median	-0.0827	0.0962	-0.860	0.3956
Interaction: LAI-273-mean* LAI-161-median	0.0909	0.0679	1.340	0.1888

*"CI" is the confidence interval. "UTC" is the untransformed coefficient. "VIF" is the variance inflation factor.

To further investigate the relationship between LAI 273 and LAI 161, I used a mean of the two LAI terms in another model. I also transformed the mean LAI term to increase the linear association with the response variable (r=0.3642, p-value = 0.0209). Yet, with a $R^2 = 0.3232$ of the resulting model (Table 5), I did not consider these models an improvement on the current five-top models listed in Table 3.

Table 5. Results of model with an averaged LAI term of LAI 273 (median) and LAI 161 (median). Model had a R2 = 0.3232 and adjusted R2 = 0.2692, and p-value <0.0011. The mean LAI term was log-transformed to improve linear association with response variable log-transformed, Hg conc.

Parameter	Coefficient	Std. Error	t-Statistic	P-Value
(Intercept)	1.4268	0.1756	8.126	<0.000
INV(HUC-10-area)	39.1111	12.0281	3.252	0.0025
INV(LAI-273-mean+ LAI-161-median]/2)	-0.7644	0.4509	-1.695	0.0984

As a final comparative test of models with these two LAI terms, I used an ANOVA to test whether the model with three variables (and potentially more collinearity) improved the model fit significantly relative to the model with only the 2 variables of HUC 10 and LAI 273 (mean). There was some significant improvement (F = 2.91, p =0.0968) of including the additional LAI-161 (median) term.

Normality of Residuals (Spatial Autocorrelation)

Moran's I test of spatial autocorrelation revealed a low probability for all five models that residuals were spatially autocorrelated (Table 6). Models 3 and 4 had p-values = 0.11, which may show some spatial autcorrelation.

Table 6. Comparison of Moran's I global test of spatial autocorrelation of regression residuals.

Model Number	Moran's Index	Expected Index	Variance	Z-score	P-value	Variables
Model 1	0.0265	-0.0256	0.0122	0.4713	0.6374	*INV(HUC-10-area) + log10(LAI-273-mean) + INV(LAI-161-median)*
Model 2	0.0898	-0.0256	0.0123	1.0420	0.2974	*INV(HUC-10-area) + log10(LAI-273-mean)*
Model 3	0.1498	-0.0256	0.0123	1.5832	0.1134	*INV(HUC-10-area) + log10(LAI-273-mean) + INV(LAI-145-median)*
Model 4	0.1498	-0.0256	0.0123	1.5832	0.1134	*INV(HUC-10-area) + log10(LAI-273-mean) + INV(LAI-161-mean)*
Model 5	0.0755	-0.0256	0.0123	0.9124	0.3616	*INV(HUC-10-area) + log10(LAI-273-mean) + INV(LAI-145-mean)*

3.3. Prediction of Hg Concentration at Unmeasured Locations

The predictions of Hg concentration are well above the observed measurements in the rest of the data Table 7. However, centering these estimates by subtracting the mean value for each model by the predicted values creates standardized and comparable prediction estimates.

Table 7. Model predictions of Hg concentration for five best models including confidence intervals.

Streamgage	Model 1		Model 2		Model 3		Model 4		Model 5	
	Pred Hg Conc.	95% CI	Pred Hg Conc.	95%CI	Pred Hg Conc.	95% CI	Pred Hg Conc.	95% CI	Pred Hg Conc.	95% CI
Sturgeon	64.63	(5.8, 715.5)	16.95	(2.7, 107.4)	34.15	(3.3, 359.2)	54.47	(4.7, 634.9)	37.81	(3.5, 407.1)
Manistique	75.03	(7.7, 733.2)	21.07	(3.7, 121.2)	43.81	(4.3, 445.9)	62.80	(6.2, 635.0)	49.47	(4.6, 527.1)
Escanaba	56.05	(5.5, 573.72)	15.68	(2.6, 95.7)	28.05	(3.2, 247.5)	47.15	(4.4, 502.2)	31.82	(3.4, 298.4)
Manistee	52.27	(5.9, 460.6)	16.11	(2.9, 88.8)	34.54	(3.4, 355.5)	43.56	(4.9, 390.3)	38.92	(3.6, 417.3)
Indian	63.19	(7.0, 571.2)	19.08	(3.4, 106.5)	43.76	(3.8, 501.1)	53.65	(5.7, 502.9)	49.32	(4.2, 583.6)
Cheboygan	57.32	(6.6, 500.0)	17.68	(3.3, 96.2)	38.37	(3.7, 398.0)	48.39	(5.4, 434.0)	43.24	(4.0, 466.7)
Thunder Bay	51.00	(5.9, 443.9)	15.84	(2.9, 86.6)	33.25	(3.4, 330.3)	43.08	(4.8, 385.5)	36.82	(3.6, 373.2)

Maumee River	115.44	(14.3, 934.1)	55.98	(8.0, 394.3)	85.44	(10.0, 728.8)	97.17	(12.2, 775.8)	94.55	(10.7, 838.0)
Raquette	62.45	(6.4, 605.5)	18.90	(3.1, 116.2)	52.54	(3.2, 861.2)	54.50	(5.3, 561.7)	58.14	(3.6, 932.9)
Mean Predicted Hg Concentration	**66.38**		**21.92**		**43.77**		**56.08**		**48.90**	

These centered values now illustrate where potentially elevated Hg concentrations could be present in the watershed. The highlighted row in Table 8 represent one streamgage in the Maumee River with elevated Hg concentration relative to the six other prediction streamagages.

Table 8. Mean-centered Hg Concentration predictions. The highlighted row represent locations that could potentially have elevated Hg concentration relative to the seven other streamgages.

Streamgage (River)	Model 1	Model 2	Model 3	Model 4	Model 5
Sturgeon	1.75	4.97	9.62	1.61	11.09
Manistique	8.65	0.85	0.04	6.71	0.57
Escanaba	10.32	6.24	15.72	8.93	17.08
Manistee	14.11	5.81	9.23	12.52	9.98
Indian	3.19	2.85	0.01	2.44	0.42
Cheboygan	9.05	4.24	5.40	7.69	5.66
Thunder Bay	15.38	6.08	10.51	13.01	12.08
Maumee River	49.07	34.06	41.67	41.08	45.65
Raquette	3.93	3.02	-8.77	1.59	-9.25

Final predictions (Figure 9) shows the distribution of predicted Hg concentration across the Great Lakes Region for the top five models. A regional pattern is present from the southern drainage basin of Maumee River to the northern Sturgeon River drainage basin.

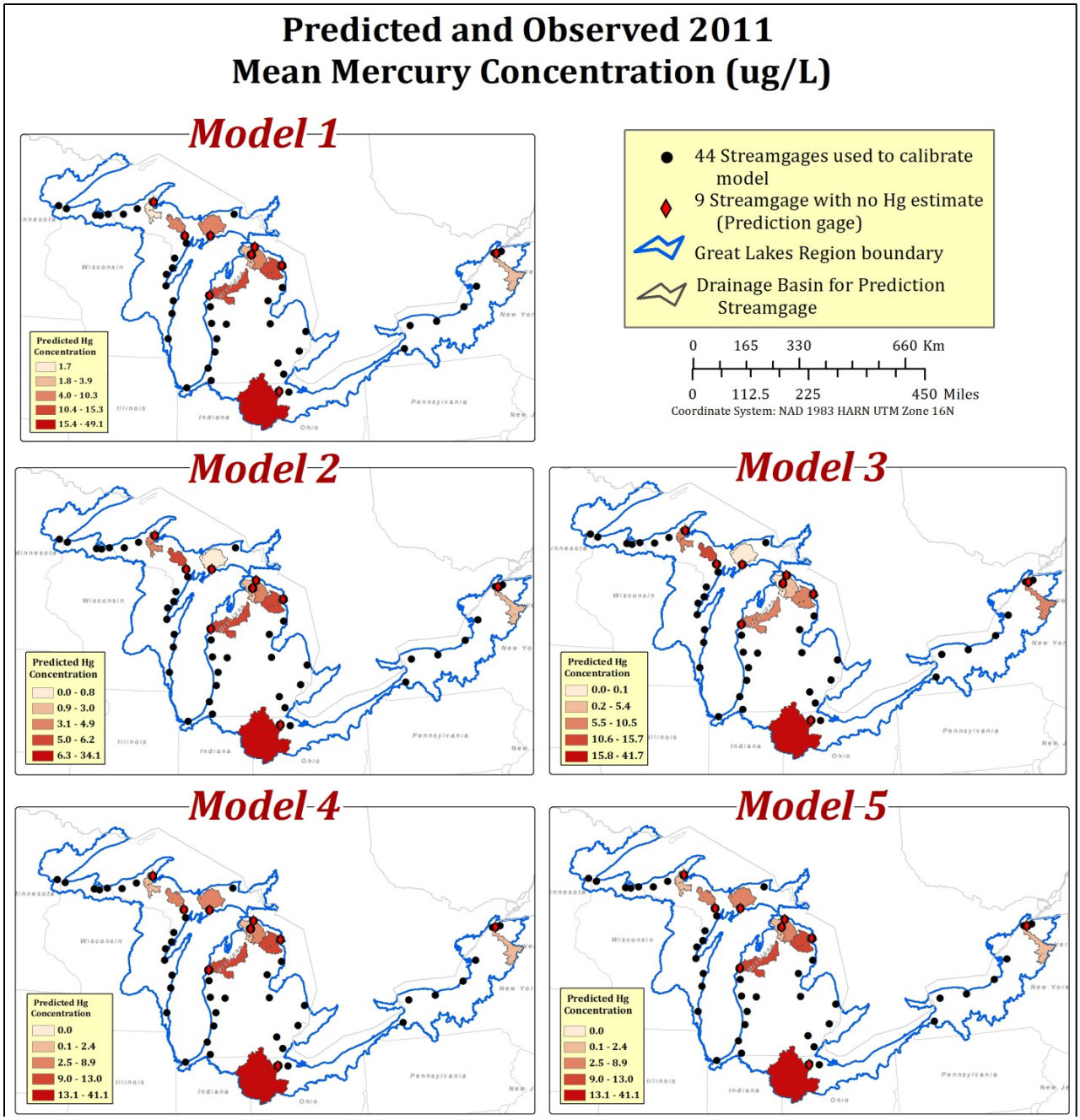

Figure 9. Displayed Hg concentration for five best models. Distributions are displayed with Jenks classes to allow comparison across all maps.

4.0. Discussion

Before the modeling, a most interesting find of this study was the negative relationship between Hg concentration and LAI. This negative relationship suggested a strong association between increased biomass and decreased Hg Concentration. This is peculiar because I originally expected a positive relationship based on the study by Risch et al. (2011) in forest watersheds that showed an increase in Hg dry deposition in areas with medium to high wet deposition. However, as Sørensen, et al., (2009) showed, increased forest cover removal leads to favorable condition for Hg methylation in the organic soils; thus causing MeHg and Hg to accumulate more readily downstream. For this paper, perhaps the negative relationship between biomass and Hg concentration reveals that the Great Lakes Region, *on average*, has high amounts of forest harvesting. However, a more in-depth analysis of site-specific fluctuations in space and time in the forest cover removal and Hg concentrations downstream could uncover local levels of biomass and Hg concentration fluctuations.

Making use of time series data for both biomass fluctuation and Hg concentrations could possibly highlight these more local variations. Alternatively, a method similar to Seitz et al. (2012) addressing forest change could identify such spatial variation. Seitz et al. (2012) assessed the influence of water quality and quantity from landscape changes including those for forest change. This basin-wide study analyzed landscape stressors and "river response" variables, revealing that forest change had strong associations with fluctuating sodium, total phosphorous, and total organic carbon.

Related to landscape patterns, to assess local clusters local patterns (e.g., elevated Hg concentration), a different spatial test is necessary. I used Moran's I, global test of spatial autocorrelation to evaluate the regression residuals. A local extension of this test known as the local indicators of spatial autocorrelation (LISAs), could evaluate spatial clustering of variables (Waller & Gotway, 2004). This may be relevant if a future study considers time series analysis of the spatial pattern of biomass and Hg concentration.

Additionally, a time series analysis using LAI terms could make use of the spatiotemporal variation of biomass as it relates to fluctuating Hg concentration. The wide confidence intervals of the Hg concentration prediction for the five top regression models may have disguised mutlicollinearity between LAI variables. Model 2, which only had the two variables of watershed area and mean LAI of Sept. 30 (Julian date 273), showed the least variance in prediction confidence intervals. The lower variance of this model without the two LAI terms also supported my original assumption that high collineaity between LAI terms would affect the model prediction.

Throughout the modeling process, I made the assumption that a smaller VIF was better to reduce the multicollinearity between predictor variables. However, as Chatterjee & Hadi (2006) noted in their text on multiple regression, a VIF of under ten is considered valid without much mutlicollinearity. Therefore, the five top models I reported in this study may have been improved by increasing the VIF value. However, I ran brief analysis with a VIF =6. This model selection process produced the same top two models. For the rest of the models, though, additional LAI terms were listed as significant, including the LAI-193 (median), LAI-139 (mean), and LAI-129 (median) models. The R^2 values for these models were very similar (e.g., $R^2 = 0.5208$ that included three LAI terms (LAI-273(median) + LAI-161 (median) + LAI-193 (median) and HUC-10 watershed area). Overall, because this short comparison still only added more LAI terms into the models, I felt confident about using the conservative VIF value (VIF = 3). Moreover, despite this collinearity

between LAI terms, the trend for three of nine prediction sites showed elevated Hg concentration an all models for the Tontogany Maumee River streamgage (Figure 9). However, given the range of prediction confidence intervals (Table 7), these results should be interpreted cautiously.

5.0. Conclusion

The affects of mercury (Hg) continue to be a persistent threat to these ecosystems, recreational activities, and economies of the Great Lakes Region. Sulfate-reducing bacteria transform Hg into methylmercury (MeHg), which can accumulate in larger piscivorous predators such as loons and fish. Humans run the risk of consuming fish with high levels of MeHg, which may lead to mental confusion, seizures, or other neurological disorders.

The distribution of Hg and the more damaging MeHg are the topic of recent research. Previous studies on the distribution of Hg highlighted the spatial variation of wet and dry Hg deposition. Identifying sources of Hg is difficult because most of Hg deposition (both wet and dry) comes from the atmosphere, traveling sometimes up to hundreds of miles. Relationships between Hg concentration and landscape attributes revealed that forest cover strongly influences nutrient fluctuation in receiving watersheds.

My project looked at predicting Hg concentration using a landscape predictor of leaf area index (LAI) from remotely sensed satellite images. I hypothesized that biomass, as an estimate of the three-dimensional canopy structure and density of forest cover would show a positive relationship with increase Hg in the receiving watershed based. However, results showed an opposite relationship, highlighting the potential local spatiotemporal variation of both Hg concentration and biomass. The final models produced highly varying predictions; yet, results did suggest a pattern of higher concentrations near urban areas. The level of forest harvesting in these areas could potentially lead to soil runoff and increased Hg levels as well. For a higher resolution study of Hg concentration, future analyses should incorporate time to detect the local variation in Hg concentration and LAI across the Great Lakes Region. Overall, this study underscores how land use change (e.g., in harvested forests or urban areas) may influence runoff of numerous contaminants, including Hg, into nearby watersheds.

6.0. Literature Cited

Ahl, D.E., Gower, S.T., Burrows, S.N., Shabanov, N.V., Myneni, R.B. and Knyazikhin, Y. (2006). Monitoring spring canopy phenology of a deciduous broadleaf forest using MODIS. *Remote Sensing of Environment*, *104,* 8895.

Arnold, N. (2010). A new approach for dealing with depression in digital elevation models when calculating flow accumulation values. *Progress in Physical Geography, 34, 6,* 781-809.

Brinda, W.D. (2012). Package 'msmv': Model selection with missing values. (R package version 1.0) [Software]. Available online at http://CRAN.R-project.org/package=msmv

Burnham, K. P. & Anderson, D.R. (2002). Lessons from the Literature and Other Matters. *Model selection and multimodal inference: a practical information-theoretic approach* (pp. 323-328) (2nd edition). New York, New York: Springer.

Buttle, J.M. & Murray, C.D. (2011). Hydrological implications of forest biomass use. Institute for Watershed Science, Final Report, Prepared for Environment Canada, Trent University, Peterborough, Ontario., 51 p.

Calcagno, V. (2012). Package 'glmulti': Model selection and multimodal inference made easy. (R package version 1.0.4) [Software]. Available online at http://CRAN.R-project.org/package=glmulti

Carter, J.M., Driscoll, D.G., and Williamson, J.E. and Lindquist, V.A. (2005). *Atlas of Water Resources in the Black Hills Area, South Dakota*. West Dakota Water Development District. U.S. Geological Survey. Hydrologic Investigations Atlas HA-747. Available online at http://pubs.usgs.gov/ha/ha747/.

Chatterjee, S. & Hadi, A.S. (2006). In Baldig, D.J., Cressie, N.A.C., Fisher, N.I., Johnstone, I.M., Kadane, J.B., Molenberghs, G., …, Teugels, J.L. (Eds.), *Regression Analysis by Example* (4th edition). Hoboken, New Jersey: John Wiley and Sons, Inc.

Cyterski, M., Galvin, M., Wolfe, K., and Parmar, R. (2012). Virtual Beach: Empirical Modeling Software for Pathogen Indicators in Recreational Beach Waters. Center for Exposure Assessment Modeling, National Exposure Research Lab - Ecosystems Research Division, Office of Research and Development, U.S. Environmental Protection Agency. (Version 2.3) [Software]. Available online at http://www.epa.gov/ceampubl/swater/vb2/vb23-dl.html.

Desrosiers, M., Planas, D., Mucci, A. (2006). Short-term response to watershed logging on biomass mercury and methylmercury accumulation by periphyton in boreal lakes. *Canadian Journal of Fisheries and Aquatic Sciences, 63,* 1734-1745.

Driscoll, C.T., Han, Y.-J., Chen, C.Y., Evers, D.C., Lampert, K.F., Holsen, T.M., Kamman, N.C., and Munson, R.K. (2007). Mercury contamination in forest and freshwater ecosystems in the northeastern united states. *Bioscience*, *57, 1,* 17.

EPA (Environmental Protection Agency). (2005). 2005 National Emissions Inventory Data and Documentation. *Technology Transfer Network Clearinghouse for Inventories and Emissions Factors.* Available online at http://www.epa.gov/ttn/chief/net/2005inventory.html.

____(2001). Emergency Planning and Community Right-to-Know Act – Section 313: Guidance for reporting toxic chemicals: Mercury and Mercury Compounds Category, Final Report EPA 260-B-01-004, Office of Environmental Information, Washington, D.C., August. Available online at http://www.epa.gov/tri/guide_docs/pdf/2001/hg2001.pdf.

____ (1995). *The Great Lakes: An Environmental Atlas and Resource Book*. Chicago, Illinois: Government of Canada, Toronto, Ontario and United States Environmental Protection Agency Great Lakes National Program Office. (3rd Edition). Available online at http://www.epa.gov/greatlakes/atlas/ .

____(1989). Great Lakes Water Quality Agreement of 1978: Protocol amending the 1978 Agreement between the United States of America and Canada on Great Lakes Water Quality as Amended on October 16, 1993. International Joint Commission, United States and Canada. Available online at http://www.epa.gov/glnpo/glwqa/1978/index.html.

Engle, M.A., Tate, M.T., Krabbenhoft, D.P., SchauerKolker, J.J., Kolker, A., Shanley, J.B., and Bothner, M.H. (2010). Comparison of atmospheric mercury speciation and deposition at nine sites across central and eastern North America, *Journal of Geophysical Research, 115*, D18306, doi:10.1029/2010JD01464.

ESRI (Environmental Systems Research Institute). (2011). ArcGIS Desktop (Version 10.0) [Software]. Redlands, California.

Evers, D.C., Wiener, J.G., Basu, N., Bodaly, R., Morrison, H.A., Williams, K.A. (2011a). Mercury in the great Lakes region: Bioaccumulation, spatiotemporal patterns, ecological risks, and policy. *Ecotoxicology*, *20*, *7,* 1487-1499.

Evers, D.C., Wiene,r J.G., Driscoll, C.T., Gay, D.A., Basu, N., Monson, B.A.,… , Soehl, A.G. (2011b). Great Lakes Mercury Connections: The Extent and Effects of Mercury Pollution in the Great Lakes Region. *Biodiversity Research Institute. Gorham, Maine. Report BRI 2011-18.* 44 p.

Fry, J., Xian, G., Jin, S., Dewitz, J., Homer, C., Yang, L., Barnes, C., Herold, N., and Wickham, J., (2011). Completion of the 2006 National Land Cover Database for the Conterminous United States, *PE&RS*, *77, 9,* 858-864.

Futter, M.N., Poste, A.E., Butterfield, D., Dillon, P.J., Whitehead, P.G., Dastoor, A.P., and Lean, D.R.S. (2012). Using the INCA-hg model of mercury cycling to simulate total and methyl mercury concentrations in forest streams and catchments. *Science of the Total Environment*, *424*, 219-231.

Gilbertson, M. and Carpenter, D.O. (2004). An ecosystem approach to the health effects of mercury in the Great Lakes basin ecosystem. *Environmental Research, 95, 240-246.*

Horizon Systems Corporation. (2012). National Hydrography Dataset Plus, version 2.0. Available online at http://www.horizon-systems.com/NHDPlus/NHDPlusV2_home.php.

Hurvichm C.M. & Tsai, C.-L. (1989), Regression and time series model selection in small samples, *Biometrika, 76*, 297-307.

Jensen, J.R. (2006). Remote Sensing of Vegetation. *Remote Sensing of the Environment: An Earth Perspective* (pp. 366-374) (2nd Edition). Upper Saddle River, New Jersey: Prentice Hall.

Jonckheere, I., S. Fleck, K. Nackaerts, B. Muys, P. Coppin, M. Weiss, F. Baret (2004), Review of methods for in situ leaf area index determination – Part I: Theories, sensors and hemispherical photography, *Agricultural and Forest Meteorology, 121*, 19-35.

Knightes, C., Sunderland, E., Barber, M., Johnston, J., and Ambrose, R. (2009). Application of ecosystem-scale fate and bioaccumulation models to predict fish mercury response times to changes in atmospheric deposition. *Environmental Toxicology and Chemistry*, *28, 4,* 881.

Knyazikhin, Y., Glassy, J, Privette, J.L., Tian, Y., Lotsch, A., Zhang, Y., …, Running, S.W. (1999). MODIS Leaf Area Index (LAI) and Fraction of Photosynthetically Active Radiation Absorbed by Vegetation (FPAR) Product (MOD15) Algorithm Theoretical Basis Document, Available online at http://modis.gsfc.nasa.gov/data/atbd/atbd_mod15.pdf.

Lindberg, S., Bullock, R., Ebinghaus, R., Engstrom, D., Feng, X., Fitzgerald, W., Pirrone, N., Prestbo, E., Seigneur, C. (2007). A synthesis of progress and uncertainties in attributing the sources of mercury in deposition. *Ambio 36,* 19-32.

Mason, R.P., Abbott, M.L., Bodaly, R.A., Bullock, O.R., Driscoll, C.T., Evers, D.C., Linderg, S.E., Murray, M., Swain, E.B. (2005). Monitoring the response to changing mercury deposition. *Environmental Science Technology 39,* 15A-22A.

Monson, B.A., Staples, D.F., Bhavsar, S.P., Holsen, T.M., Schrank, C.S., Moses, S.K., McGoldrick, D.J., Backus S.M., Williams, K.A. (2011). Spatiotemporal trends of mercury in walleye and largemouth bass from Laurentian Great Lakes region, *Ecotoxicology Special Issue.*

Moran, P.A.P. (1950). Notes on continuous stochastic phenomena. *Biometrika, 37,* 17-23.

Murray, C.D. & Buttle, J.M. (2003). Impacts of clearcut harvesting on snow accumulation and melt in a northern hardwood forest. *Journal of Hydrology, 271,* 197-212.

Myneni, R., Knyazikhin, Y., Glassy, J., Votava, P. and Shabanov, N. (2003). User's Guide FPAR, LAI (ESDT: MOD15A2) 8-day Composite NASA MODIS Land Algorithm. *Terra MODIS Land Team.* Available online at http://cybele.bu.edu/modismisr/products/modis/userguide.pdf.

NASA (National Aeronautics and Space Administration). (2011). MODIS (Moderate Resolution Imaging Spectroradiometer), MOD 15 - Leaf Area Index (LAI) and Fractional Photosynthetically Active Radiation (FPAR). Available online at http://modis.gsfc.nasa.gov/data/dataprod/dataproducts.php?MOD_NUMBER=15.

Neitsch, S.L. Arnold, J.G., Kiniry, J.R., and Williams, J.R. (2011). Soil and Water Assessment Tool: theoretical documentation. (Version 2009). Texas A&M University System, Grassland, Soil, and Water Research Laboratory, and Agriculture Research Service Blackland Research Center, and Texas AgriLife Research. Texas Water Resources Institute Technical Report No. 406.

Pena, E.A. & Slate, E.H. (2006). Global validation of linear model assumptions, *Journal of American Statistical Association*, 101, 473, 341-354.

R Core Team. (2012). R: A language and environment for statistical computing. R Foundation for Statistical Computing, Vienna, Austria. ISBN 3-900051-07-0. (Version 2.15) [Software]. Available online at http://www.R-project.org/.

Risch, M.R., Dewild, J.F., Krabbenhoft, D.P., Kolka, R.K., Zhang, L. (2011). Litterfall mercury deposition in the eastern USA, *Environmental Pollution Special Issue.*

Schäuble, H., Marinoni, O., and Hinderer, M. (2008). A GIS-based method to calculate flow accumulation by considering dams and their specific operation time. *Computer and Geosciences, 34, 6*, 635-646. Availabl online at http://dx.doi.org/10.1016/j.cageo.2007.05.023.

Schwartz, G.E., Hoos, A.B., Alexander, R.B., Smith, R.A. (2006). The SPARROW surface water-quality model: theory, applications and user documentation. US Geological Survey Techniques and Methods Reports, Book 6, Chapter B3.

Seitz, N.E., Westbrook, C.J., Dube, M.G., and Squires, A.J. (2012). Assessing large spatial scale landscape change effects on water quality and quantity response in the lower Athabasca River basin. *Integrated Environmental Assessment and Management, Special Series,* 1551-3793. Available online at http://dx.doi.org/10.1002/ieam.1336.

Silbernagel, S.M., Carpenter, D.O., Gilbert, S.G., Gochfeld, M., Groth III, E., Hightower, J.M., and Schiavone, F.M. (2011). Recognizing and Preventing Overexposure to Methylmercury from Fish and Seafood Consumption: Information for Physicians, *Journal of Toxicology 2011,* Article ID 983072, 7 p, doi:10.1155/2011/983072.

Søreson, R., Meili, M., Lambertson, L., von BrÖmssen, C., and Bishop, K. (2009). The effects of forest harvest operations and methymercury in two boreal streams: relatively small changes in the first two years prior to site preparation. *Ambio, 38,* 364-372.

Tobler W. (1970). A computer movie simulating urban growth in the Detroit region. *Economic Geography*, *46,2,* 234-240.

UNEP Chemical Branch (United Nations Environment Program Chemical Branch). (2008). The global atmospheric mercury assessment: sources, emissions, and transport, *United Nations Environment Programme, Geneva, Switzerland.* Available online at http://www.unep.org/hazardoussubstances/LinkClick.aspx?fileticket=Y0PHPmrXSuc%3d&tabid=3593&language=en-US .

US Bureau of the Budget. (1947). US National Map Accuracy Standards. Available online at http://nationalmap.gov/standards/pdf/NMAS647.PDF.\

USGS & EPA (US Geological Survey and Environmental Protection Agency). (2012). National Hydrography Dataset (Great Lakes Region). Available online at http://nhd.usgs.gov

USGS NSIP (US Geological Survey, National Streamflow Information Program). (2010). Number of USGS Streamgages through Time. USGS Office of Surface Water Quality. Available online at http://water.usgs.gov/nsip/history1.html.

USGS & USDS NRCS (US Geological Survey and US Department of Agriculture, Natural Resources Conservation Service). (2012). Federal Standards and Procedures for the National Watershed Boundary Dataset (3rd edition.): U.S. Geological Survey Techniques and Methods 11–A3 (pp. 63). Available online at http://pubs.usgs.gov/tm/tm11a3/.

Waller, L.A. & Gotway, C.A. (2004). Spatial Clustering of Health Events: Regional Count Data. In Baldig, D.J., Cressie, N.A.C., Fisher, N.I., Johnstone, I.M., Kadane, J.B., Molenberghs, G., …, Teugels, J.L. (Eds.), *Applied Spatial Statistics for Public Health Data.* Hoboken, New Jersey: John Wiley and Sons, Inc.

Winkler, R.D., Boon, S., Zimonick, B., and Baleshta, K. (2010). Assessing the effects of post-pine beetle forest litter on snow albedo. *Hydrologic Processes, 24,* 803-812.

Winkler, R.D., Spittlehouse, D.L., and Golding, DL. (2005). Measure of differences in snow accumulation and melt among clearcut, juvenile and mature forests in southern British Columbia. *Hydrological Processes, 19,* 51-62.

Yang, B.T., Huang, D., Rautiainen, M., Shabanov, N.V., Wang, Y., Privette, J.L., …, and Myneni, R.B. (2006). MODIS Leaf Area Index Products: From Validation to Algorithm Improvement. *IEEE Transactions on Geoscience and Remote Sensing, 44(7),* 1885-1898.

Zheng, G. & Moskal, M. (2009). Retrieving leaf area index (LAI) using remote sensing: theories, methods and sensors, *Sensors, 9,* 2719-2745, doi:10.3390/s90402719.

7.0 Appendix: Five best-fit models for predicting Hg concentration in the Great Lakes Region.

A.1. Model 1

Parameter	Coefficient	95% CI*	Std. Error	t-Statistic	P-Value	Standardized Coefficient	UT Coef*	95% CI Interval (UT Coef)	VIF
(Intercept)	3.482	(2.161, 4.802)	0.651	5.347	<0.000				
INV(HUC-10-area)	43.640	(22.094, 65.187)	10.623	4.108	<0.000	0.507	0.023	(0.045, 0.015)	1.071
log10(LAI-273-mean+1)	-1.870	(-2.892, -0.847)	0.504	-3.71	0.001	-0.676	0.014	(0.001, 0.142)	2.439
INV(LAI-161-median)	-0.312	(-0.682, 0.059)	0.183	-1.705	0.097	-0.318	-3.208	(-1.466, 16.954)	2.331

*"CI" is the confidence interval. "UTC" is the untransformed coefficient. "VIF" is the variance inflation factor.

A.2. Model 2

Parameter	Coefficient	95% CI*	Std. Error	t-Statistic	P-Value	Standardized Coefficient	UT Coef*	95% CI (UT Coef)	VIF
(Intercept)	2.600	(1.778, 3.423)	0.406	6.404	<0.000				
INV(HUC-10-area)	39.353	(17.906, 60.800)	10.585	3.718	<0.000	0.457	0.025	(0.001, 0.029)	1.011
log10(LAI-273-mean+1)	-1.222	(-1.912, -0.532)	0.3404	-3.589	0.001	-0.442	0.01	(0.056, 0.016)	1.011

*"CI" is the confidence interval. "UTC" is the untransformed coefficient. "VIF" is the variance inflation factor.

A.3. Model 3

Parameter	Coefficient	95% CI*	Std. Error	t-Statistic	P-Value	Standardized Coefficient	UT Coef*	95% CI (UN Coef)	VIF
(Intercept)	3.277	(1.647, 4.907)	0.804	4.078	<0.000				
INV(HUC-10-area)	39.023	(17.531, 60.516)	10.597	3.682	0.001	0.454	0.026	(0.057, 0.017)	1.012
log10(LAI-273-mean+1)	-1.669	(-2.828, -0.511)	0.571	-2.922	0.006	-0.603	0.214	(0.001, 0.031)	2.842
INV(LAI-145-median)	-0.258	(-0.795 , 0.278)	0.265	-0.976	0.336	-0.201	-3.875	(-1.259, 3.593)	2.824

*"CI" is the confidence interval. "UTC" is the untransformed coefficient. "VIF" is the variance inflation factor.

A.4. Model 4

Parameter	Coefficient	95% CI*	Std. Error	t-Statistic	P-Value	Standardized Coefficient	UT Coef*	95% CI (UT Coef)	VIF
(Intercept)	3.387	(2.012 , 4.761)	0.678	4.996	<0.000				
INV(HUC-10-area)	42.579	(20.930, 64.227)	10.674	3.988	<0.000	0.495	0.024	(0.048, 0.016)	1.057
log10(LAI-273-mean+1)	-1.792	(-2.846, -0.738)	0.520	-3.449	0.002	-0.648	0.002	(0.001, 0.018)	2.42
INV(LAI-161-mean)	-3.226	(-7.777, 1.325)	2.244	-1.438	0.159	-0.275	-0.310	(-0.129, 0.755)	2.512

*"CI" is the confidence interval. "UTC" is the untransformed coefficient. "VIF" is the variance inflation factor.

A.5. Model 5

Parameter	Coefficient	95% CI*	Std. Error	t-Statistic	P-Value	Standardized	UT Coef*	95% CI (UT	VIF

						Coefficient		Coef)	
(Intercept)	3.359	(1.719, 5.00)	0.809	4.153	<0.000				
INV(HUC-10-area)	39.628	(18.205, 61.050)	10.56	3.752	0.001	0.461	0.025	(0.055, 0.016)	1.011
log10(LAI-273-mean+1)	-1.735	(-2.916, -0.554)	0.582	-2.98	0.005	-0.627	0.002	(0.001, 0.028)	2.972
INV(LAI-145-mean)	-0.310	(-0.890, 0.270)	0.2860	-1.084	0.285	-0.228	-3.225	(-1.124, 3.706)	2.969

*"CI" is the confidence interval. "UTC" is the untransformed coefficient. "VIF" is the variance inflation factor.